Received: 9 May 2018 | Revised: 13 December 2018 | Accepted: 13 December 2018
DOI: 10.1002/rcs.1981

WILEY The International Journal of Medical Robotics and Computer Assisted Surgery

ORIGINAL ARTICLE

The MUSHA underactuated hand for robot-aided minimally invasive surgery

Mario Selvaggio[1] | Giuseppe Andrea Fontanelli[1] | Vincenzo Romano Marrazzo[1] | Umberto Bracale[2] | Andrea Irace[1] | Giovanni Breglio[1] | Luigi Villani[1] | Bruno Siciliano[1] | Fanny Ficuciello[1]

[1]Department of Information Technology and Electrical Engineering, University of Naples Federico II, Naples, Italy
[2]Department of Public Health, University of Naples Federico II, Naples, Italy

Correspondence
M. Selvaggio, Department of Information Technology and Electrical Engineering, University of Naples Federico II, via Claudio 21, 80125 Naples, Italy.
Email: mario.selvaggio@unina.it

Funding information
MUSHA, Grant/Award Number: 320992

Abstract

Background: Keyhole surgery is characterized by loss of dexterity of surgeon's movements because of the limited workspace, nonintuitive motor skills of the surgical systems, and loss of tactile sensation that may lead to tissue damage and bad execution of the tasks.

Methods: In this paper, a three-fingered underactuated miniature tool for robot-aided laparoscopic surgery is presented. The design is conceived to realize a closed-hand configuration allowing the insertion of the tool into the abdominal cavity through the trocar in one step and to reach different grasping as well as pushing/holding configurations once in the cavity.

Results: Aiming to replicate human hand dexterity and versatility, different solutions for the kinematic structure of the hand are analyzed using quality indices to evaluate the manipulability and stability of the grasp. Furthermore, a first prototype of fingertip force sensor based on fiber Bragg grating (FBG) technology has been realized and tested. The design choices of the prototype are described and discussed with the aid of experiments.

Conclusions: The whole concept and the need for such anthropomorphic tool are discussed with surgeons to highlight constraints and potentials in surgical tasks. The feedback by expert surgeons is used to provide specifications and improvements to the kinematics and mechanical design. The investigations of different designs allow identifying the optimal solution to improve grasping and manipulation capabilities. The tests on FBG sensors led to the conclusion that this technology guarantees good performance and can be a good solution for applications in surgical robotics.

1 | INTRODUCTION

Laparoscopic robotic surgery, and in general, minimally invasive surgery (MIS), has obvious advantages compared with the traditional open surgery. The main advantages, for which in the last decade robotics has taken a key role, are the minimized postoperative pains, speed-up of the recovery time, increased comfort for the surgeon, improved performance, reduced hemorrhaging, and reduced risk of infections. Besides advantages, significant drawbacks of keyhole surgery are the loss of dexterity of surgeon's movements due to the limited range of motion and non-intuitive motor skills of surgical systems and, finally, the loss of tactile sensation leading to tissue damage and bad execution of tasks like suturing. Consequently, experience and ability of the surgeon make the difference. The use of robots aims at overcoming these limitations. Nevertheless, the ordinary forceps used in robotic systems, like in the da Vinci robot, have limited dexterity and lack of sensors to measure interaction forces. Therefore, traditional laparoscopic surgery is affected by the need for new instruments to facilitate surgical maneuvers. The possibility to have a surgical instrument that can gently manipulate the bowel and keep it located in the upper abdomen would be of great help for surgeons. Moreover, the sense of touch is essential to allow humans to derive information about their surroundings when other senses are not appropriate to distinguish between a variety of physical stimuli, including temperature, pressure, and texture. This work contributes to fostering the adoption of artificial hands in the surgical field where the use of anthropomorphic prehensile devices can make the difference. Besides humanoid robots and prosthetics applications, other areas such as minimally

invasive laparoscopic surgery could benefit by the use of suitably designed hands able to enter the patient's body through the trocar and to replace the hands of the surgeon by equaling dexterity and sensory ability at the same time. Because of the presence of multiple degrees of freedom (DoFs), a synergistic approach inspired by the human hand is adopted for the design. This device has a high number of DoFs to allow complex and human-like motions but, at the same time, is controlled with a lower number of signals, hence using few motors. The paper is organized as follows. In Section 2, a state of the art of related works are provided and the innovative insight of the proposed tool is highlighted. Section 3 describes the constraints and potentials of the tool from the surgeons' point of view. In Section 4, different kinematics solutions are evaluated and compared, while Section 5 describes the solution adopted for the tip force sensors. Section 6 describes the MUSHA prototype; and finally, Section 7 sketches future perspectives and conclusions.

2 | RELATED WORKS

The need of a hand-like tool for laparoscopic surgery is demonstrated by the existence of a hand-assisted laparoscopic surgery (HALS) technique,[1] where the operator's hand is inserted through a small incision into the abdomen. This technique has the advantage of providing the surgeons with capabilities of exposure, traction, palpation, tactile sensation, and digital dissection of the operative specimen while the operative field is visualized as in standard laparoscopic surgery, namely with a video monitor. Besides the advantages, the applications of HALS have been limited to a few major centers. This is because instruments suitable for HALS are limited to few standard operative ones. Indeed, open issues are related to: (a) operator fatigue, (b) potential risk for injury to other organs, (c) need of suitable setup for HALS that requires appropriate operating table height and orientation, and (d) optimized positioning of the operating ports to avoid that the assisting hand is too close or too far from the target organ. Indeed, in the first case, the hand could obscure vision while, in the second case, it could cause surgeon fatigue.

MUSHA aims at finding a suitable trade-off between the use of standard laparoscopic forceps and the HALS technique by introducing the advantages of anthropomorphic manipulation capabilities in the da Vinci setup.

Several works available in the literature are dedicated to improving the dexterity of surgical tools and to provide forceps with force measurements. Most of them are devoted to surgical manipulators design. In Ikuta, Hasegawa, and Daifu's study,[2] a new robotic system named "Hyper Finger" for MIS has been developed. The complete system provides multiple fingers as separated manipulators that enter in the abdomen through different ports. Each finger has nine DoFs and has a diameter of 10 mm. In Cavusoglu, Williams, Tendick, and Sastry's study,[3] a telesurgical system with millimeter-scale robotic manipulators is introduced. In the study of Lum et al,[4] seven different minimally invasive surgical tasks from 30 surgeons are acquired to design a kinematic optimization of a seven-DoF cable-actuated spherical surgical robotic manipulator. In Tzemanaki, Walters, Pipe, Melhuish, Dogramadzi's study,[5] starting from a survey conducted among surgeons regarding their opinion on surgical training and surgical systems, a three-fingered surgical hand with shape memory alloy (SMA) helix actuators has been realized with a diameter of 18 mm and controlled using an exoskeleton as a master manipulator. In this way, the motion mapping from the surgeon's hand is intuitive and straightforward. In Luo and Wang's study,[6] a 10-DOF robotic metamorphic instrumental hand has been developed for MIS and controlled with a master glove. The hand can be inserted into the patient abdomen cavity through a port with a diameter of 24 mm. Compared with the cited surgical hands, the MUSHA hand (MH) has an innovative design that allows a diameter of 15 mm. The kinematics has 11 DoFs with an underactuated solution that maximizes dexterity and grasp stability. Last but not least, a solution for the force sensor on the tip is designed and tested with promising results for further developments.

3 | CONSTRAINTS AND POTENTIALS IN SURGICAL TASKS

Nowadays, MIS represents the gold standard approach in many surgical procedures useful for the treatment of abdominal benign and malignant diseases. Since the 90's, laparoscopic surgery (LS) has gained wide acceptance among the surgeons for the treatment of gastrointestinal diseases as well as colon cancer, gallbladder disease, functional gastroesophageal disorders, and cancer.[7,8] However, LS has many constraints such as straight instruments, poor 3D vision sometimes associated with motion sickness, instruments clashing, and limited haptic feedback. These limitations determine trouble during the learning curve of LS, reducing the spread of this approach. At the beginning of the 2000s, robotic surgery (RS) has been introduced as a new approach in MIS with the aim of overcoming the limits of LS. In many fields, it quickly replaced the LS such as urological procedures, pancreatic and liver surgery, and rectal surgery.[9]

The advantages of RS are the use of articulated instruments, a better 3D vision, an enhanced dexterity, and a greater visual with consequent better precision. However, the actual generation of instruments overlaps the laparoscopic ones. In the last years, the development of robotic instruments focused on the adaptation of existing laparoscopic tools to RS.

The MH represents one of the first examples of a new concept that tries to replicate the natural hand movements. This feature could be very useful to enhance the traction and counter-traction relationship during the dissection maneuver. Moreover, the grasp can be more efficient and less traumatic on the bowel during a colorectal procedure. In the same way, according to a multitasking concept, MH could be used as a retractor of different organs (bowel, solid organ muscles, etc). For example, in a hiatal hernia repair, MH could be useful as a hepatic retractor, as well as it can serve as an instrument passing under the esophagus during the periesophageal fundoplication.[10]

Moreover, the surgical hand could be more performing than the actual forceps in the maneuver of rectal dissection from the prostate during robotic anterior resection.[11] However, the current configuration has some limitation. The instrument diameter of 15 mm needs the use of a bigger port with respect to the current one. Another issue is that the actual robotic console does not allow the telemanipulation of the three fingers. Anyhow, future developments of MH will overcome these limitations.

Further potentials are here described. For example, because of the knowledge of kinematics, the hand can be used as a caliper, obtaining precisely the dimensions of wall defect during an abdominal wall reconstruction rather than to calculate the appropriate distance of bowel section from a tumor. Also, MH could be used for organ/tissues palpation to retrieve information about the organ consistency to discern, for example, between stools and polyps in the bowel. Moreover, it is conceivable that the association of MH to bipolar energy or radio frequency to gain an additional instrument for hemostasis could be very useful during bloody procedures like hepatic or partial kidney resections.

4 | ANALYSIS OF DIFFERENT KINEMATICS SOLUTIONS

For guaranteeing human-inspired manipulation capabilities, the robotic hand should have a number of DoFs comparable with that of the human hand. However, neuroscientific studies have demonstrated that, in the human hand, joint angles do not vary independently: for a given task, the hand posture is regulated by few postural synergies.[12] A principal components analysis showed that the first two components account for more than 80% of the variance for grasping tasks. This result permits to substantially reducing the complexity of the grasp synthesis and control. In our work, taking inspiration from this paradigm, we have chosen to develop a three-fingered 11-DoFs mechanism actuated by four motors. This choice allows keeping human-like dexterity in the mechanism while complying with the restrictions introduced by the underactuation, like in the da Vinci Research Kit instrument interface. In this section, we analyze three possible solutions involving different joint couplings (in the following, we refer to these joint couplings as mechanical synergies or simply synergies).

Underactuation can be mathematically described by the mechanical synergies matrix S that relates motor velocities $\dot{\boldsymbol{z}} = \left[\dot{z}_1, \dot{z}_2, \ldots, \dot{z}_{n_z}\right]$ and joint velocities $\dot{\boldsymbol{q}} = \left[\dot{q}_1, \dot{q}_2, \ldots, \dot{q}_{n_q}\right]$ usually in a linear fashion: $\dot{\boldsymbol{q}} = S\dot{\boldsymbol{z}}$, with n_z and n_q being the number of actuators and the number of joints, respectively. In the following, we consider the vector $\boldsymbol{q}$ composed of the joint variables of the thumb, index, and middle ordered from metacarpal to distal joints. That said, to establish which mechanical constraints in the motion transmission system gives the overall best performance for all the given task requirements, we analyzed and compared different solutions. The three S matrices shown below realize different joint couplings

$$S_1 = \begin{bmatrix} \boldsymbol{a} & 0 & 0 & \boldsymbol{b} \\ 0 & 0 & 0 & 0 \\ 0 & \boldsymbol{a} & 0 & \boldsymbol{b} \\ 0 & 0 & 0 & 0 \\ 0 & 0 & \boldsymbol{a} & \boldsymbol{b} \end{bmatrix} S_2 = \begin{bmatrix} \boldsymbol{a} & 0 & \boldsymbol{b} & 0 \\ 0 & 0 & 0 & 0 \\ 0 & \boldsymbol{a} & 0 & \boldsymbol{b} \\ 0 & 0 & 0 & 0 \\ 0 & \boldsymbol{a} & 0 & \boldsymbol{b} \end{bmatrix} S_3 = \begin{bmatrix} 1.0 & 0 & 0 & 0 \\ 0 & \boldsymbol{a} & 0 & \boldsymbol{b} \\ 0 & 0 & 0 & 0 \\ 0 & 0 & \boldsymbol{a} & \boldsymbol{b} \\ 0 & 0 & 0 & 0 \\ 0 & 0 & \boldsymbol{a} & \boldsymbol{b} \end{bmatrix}, \quad (1)$$

where $\boldsymbol{a} = [1.00, -0.30, -0.21]^{\mathsf{T}}$, $\boldsymbol{b} = [0, 1.00, 0.70]^{\mathsf{T}}$.

Notice that S_1 matrix implements a solution in which all the metacarpal joints are uncoupled, while all the other DoFs are coupled and have human-like joint proportions.[13]

Conversely, the S_2 matrix represents a solution in which the thumb joints are completely uncoupled from the other fingers. The S_3 matrix is similar to S_1 but with the metacarpal joints of the index and middle fingers coupled. Thus, there is one unused motor, and the matrix presents an additional row corresponding to a q_0 DoF that accounts for the presence of a wrist mechanism located at the base of the hand.

The mathematical model of the hand-object system constrained in a grasp configuration helps to study the capabilities embodied in the mechanism. Following the approach in Prattichizzo, Malvezzi, Gabiccini, and Bicchi's study,[14] we seek to analyze the controllable internal forces, rigid-body object motion, and potential hand redundant motions. It is possible to show that the following relations between object displacements Δu, contact forces $\Delta\lambda$, and synergies actuation Δz hold

$$\Delta u = \left(GKG^{\mathsf{T}}\right)^{-1} GKJS\Delta z = V\Delta z, \quad (2)$$

and

$$\Delta\lambda = \left(I - G_K^{\dagger}G\right) KJS\Delta z = P\Delta z, \quad (3)$$

where G is the grasp matrix, $G_K^{\dagger}$ is the weighted right pseudoinverse of G, K is the symmetric and positive definite matrix of the equivalent stiffness at the contact, J is the block diagonal Jacobian matrix, and S the mechanical synergies matrix. For more details on the derivation of grasp and Jacobian matrices, the reader can refer to Prattichizzo and Trinkle's study.[15] For simplicity, the expressions of matrices P, V, and K summarized here are those obtained by neglecting the so-called geometric effects, arising from the linearization, and depending on J matrix variability with respect to the hand and object configuration. Hence, the set of controllable active internal forces $\Delta\lambda$ can be expressed as

$$\Delta\lambda = E_s\alpha, \quad (4)$$

where

$$\mathcal{R}\left(E_s\right) = \mathcal{R}\left(\left(I - G_K^{\dagger}G\right) KJSY\right), \quad (5)$$

being $\mathcal{R}(\cdot)$ the range or column space of the matrix in the argument and $\alpha \in \mathbb{R}^e$ is a vector parameterizing the solution. An optimal choice $\hat{\alpha}$ can be derived by means of suitable cost functions and optimization routines.

Complementary, the set of rigid-body motions that do not involve deformations in the contact points and that are controllable by activating the synergies can be derived by imposing $\Delta\lambda = 0$ in the object equilibrium equation,[14] namely $w + G\lambda = 0$, where w is the load on the object. The rigid body motion thus belongs to the null space $\mathcal{N}([JS - G^{\mathsf{T}}])$.

We can then define a matrix Γ, whose columns form a basis of such null space. Under the hypothesis that the object motion is nor indeterminate neither redundant, Γ can be expressed as

$$\Gamma = \mathcal{N}[JS - G^{\mathsf{T}}] = \begin{bmatrix} \Gamma_{zcs} \\ \Gamma_{ucs} \end{bmatrix}, \quad (6)$$

where the coordinated rigid-body motions of the hand and those of the object belong to the range spaces of Γ_{zcs} and Γ_{ucs}, respectively. It is easy to show that

$$\mathcal{R}\left(\Gamma_{ucs}\right) \subseteq \mathcal{R}\left(\left(GKG^{\mathsf{T}}\right)^{-1} GKJSY\right), \quad (7)$$

i.e., the rigid body motions of the objects are a subset of all synergy-controlled object motions that also contain motions due to the elastic deformations.

4.1 | Kinematic evaluation

In this section, we present a comparison that aims at evaluating the hand's grasping and manipulation capabilities in terms of optimized forces and allowed movements of the three different solutions.

First, we evaluate the force-closure cost function,[16] computed using Syngrasp toolbox,[17] for a given set of object poses along trajectories planned in the reachable workspace of the three kinematics solutions. It is worth recalling that the minimum of the cost represents the best grasp feasible with the given set of synergies.

Two trajectories of object poses have been considered: one along z direction, and one along a circumference arc in the yz plane (see Figure 1, where the reference frame is represented in the images on the left). The path along z starts at $z_i = 30$ mm and ends at $z_f = 40$ mm measured in the palm reference frame, while the path in the yz plane is an arc of radius $r = 45$ mm and $\theta_i = 77^\circ, \theta_f = 108^\circ$.

The results are shown in Figure 1. The force closure cost function has been computed assuming a friction coefficient $\mu = 0.5$, a minimum value of the normal force $\lambda_{min} = 0.1$ N and a maximum value $\lambda_{max} = 5$ N, and an external load on the object $w = [0, 0, 1, 0, 0, 0]$. The S_1 kinematic solution has smaller costs with respect to the other solutions in both the planned paths.

Figure 1 also contains an example of the principal direction of motion of the object in Cartesian space calculated according to (7) for the S_1 (top) and S_2 (bottom) hands. We have found that the column space of Γ in (7) has dim $= 1$ for the hand having S_1 couplings and dim $= 2$ for the hand having S_2 and S_3 couplings. This means that the hand S_1 can realize one object movement along z-axis, S_2 can move the object in the yz plane, while S_3 in the xz plane, due to the presence of the wrist. Therefore, S_2 and S_3 present better manipulability with respect to the solution S_1.

The results presented here are theoretical findings that are valid when the contact force does not vary. However, some trajectories of the object in Cartesian space can still be accomplished if we remove this hypothesis. Thus, we have performed a second set of experiments for evaluating the Cartesian space error introduced by the kinematic couplings along a given desired trajectory of the object.

Three trajectories have been considered: pure translation along z-axis, pure translation along y-axis, and pure rotation about x-axis centered in the object. These have been chosen by looking at the potential tasks to be performed by the hand.

Figure 2 contains the error with respect to the desired trajectory. The error is produced by the approximation in the inverse kinematics

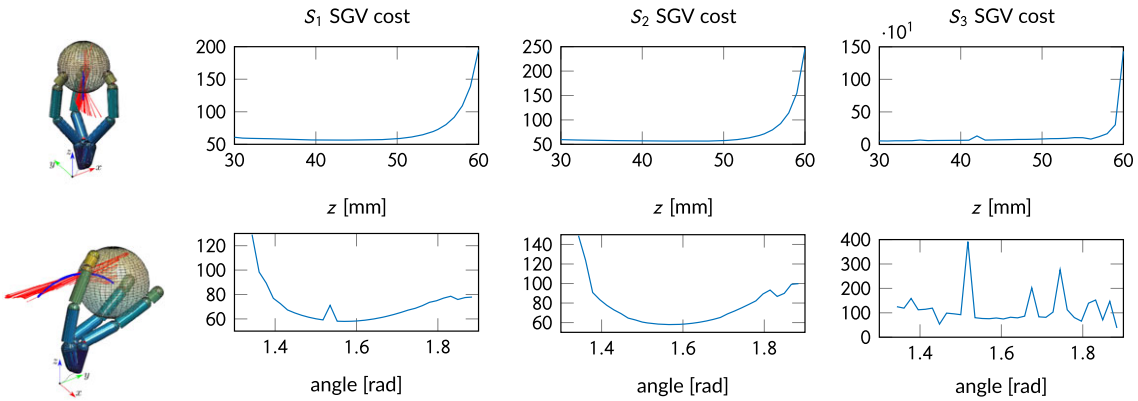

FIGURE 1 SGV cost variations: along z direction (top) and along the circular path on yz plane with respect to the rotation angle (bottom). The red lines on the left are the principal directions of motion

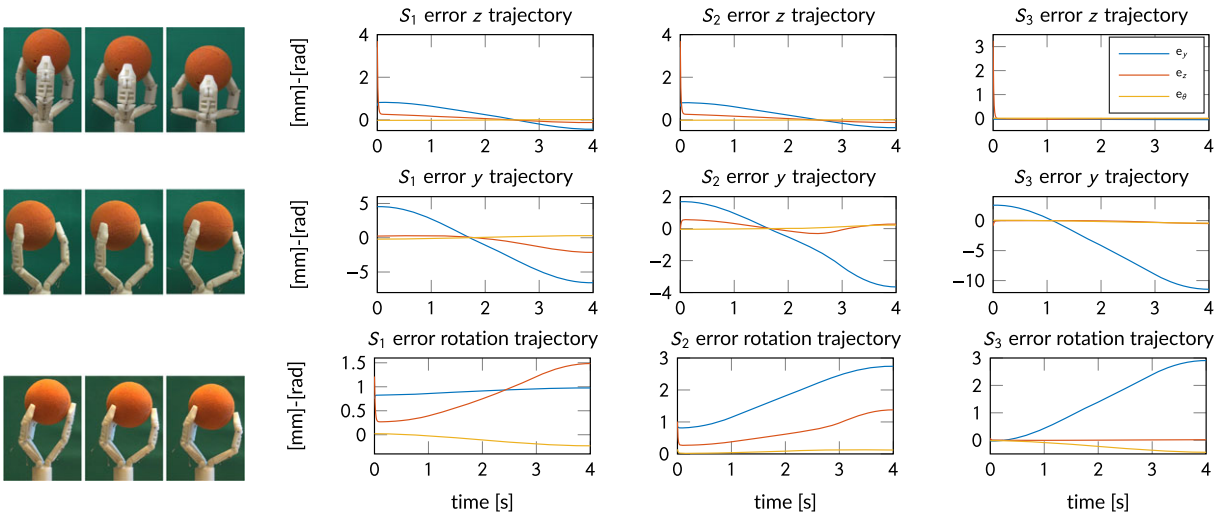

FIGURE 2 Object errors in the Cartesian space for S_1, S_2, and S_3 for three different trajectories: along z direction, along y direction, and for the rotation in the yz plane. The left pictures are taken from real experiments performed on the prototype implementing S_1 coupling matrix

due to the underactuation. In these experiments, we suppose that the motion implying rolling is small enough so that the contact points do not change over time in the object reference frame. The rotation error has been calculated as the angle, about x-axis, between the plane containing the fingertips and a fixed horizontal plane. The z trajectory starts at $z_i = 40$ mm and ends at $z_f = 20$ mm, The y trajectory starts at $y_i = -5$ mm and ends at $y_f = 20$ mm measured in the palm reference frame, while the rotation is of $\theta = -25^\circ$ evaluated in the object reference frame. The plots show that only the z trajectory is performed with a small tracking error, since the desired path is planned in the hand workspace. Therefore, the inverse kinematics computed using the Jacobian transpose provides a solution with a small error.

Overall, we can say that the rotational trajectory is better tracked by S_1 at the cost of higher errors on the other two axes. S_2 has the minimum error norm. The y trajectory is better performed by S_2, while the z trajectory is better tracked by S_3. As a final remark, we can say that S_1 solution is better to stably grasp objects while S_2 presents better performance in moving the objects but still presents SGV costs comparable with that of the S_1 solution. According to these preliminary results, S_2 is the best solution.

4.2 | Comparison with a standard laparoscopic instrument in a simulated environment

In this section, we present a comparison of MH with respect to standard tools. The aim is to evaluate MH potential in selected tasks during adrenalectomy and colectomy procedures. The simulated tasks are organs mobilization, grasping, and measuring of critical dimensions of affected organs.

Since the MH is still a prototype, not ready to be tested in surgical environments, the proof of concept is obtained by moving our tool in a simulated environment. A qualitative evaluation is performed by replicating in simulation the execution of real tasks with standard laparoscopic tools. Figure 3 presents the simulation environment. The dVRK and MH simulator are realized using V-REP.[18,19] The choice is motivated by the versatility and simplicity of this software for multi-robot applications.

In our experimental setup, we use bullet physics engine to simulate the interaction between the MH and a soft organ. The soft organ is simulated using a soft triangular mesh shape with elastic properties.[20] The organ is anchored to the rigid scene in different points to simulate the interaction with the abdominal surfaces. The MH is rendered using three spheres for each finger simulating the hand phalanges. We have linked the bullet scene to our VREP simulator through remote API functions to have at each time step the position of each hand phalanges w.r.t. the robot Remote Center of Motion (RCM).

In Figure 4, MH is used in retractor configuration to lift and mobilize organs to facilitate surgical intervention. This can be the case of the adrenal gland during adrenalectomy procedure. The advantage of MH is to provide an extended contact area, force distribution, and thus more gentle and effective maneuvers. As shown in the top images of Figure 4, standard tools are improperly used as retractor by exploiting contact between the shaft and the organ. The motivation is to enlarge the contact area since the forceps are not suitable for holding and raising extended surfaces. There are tools designed to perform this role (retractors) but they should be continually replaced and this is clearly impossible in the context we are observing. Therefore, to cope with this issue, the surgeon used thin cylindrical shafts, which do not guarantee stable contact and grip, and which can lead to more tissues stress. The advantage of MH is that it includes several functions and configurations in a single tool, avoiding the need to replace it continuously.

In Figure 5, MH is used as a grasper to grab organs or tissues. The presence of articulations and of three fingers endowed with force sensors allows grasping with increased flexibility respect to different organ/tissues dimensions and locations, and with increased stability while reducing stress and damages of the affected organs. Grasping and manipulation abilities of MH constitute a great potential in diagnosis. Thanks to force sensing, MH is an extension of the surgeon in all respects. In fact, the hand can be used as a means of palpation to touch and feel tissues and organs, and therefore can

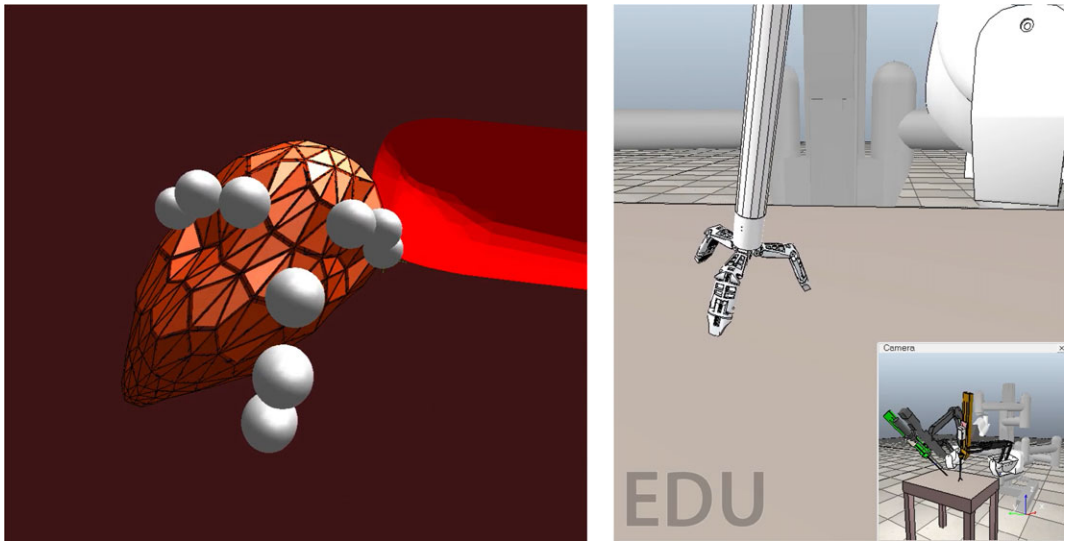

(A) (B)

FIGURE 3 Simulation environment of the MH mounted on the da Vinci robot. A, Bullet scene; B, V-REP environment

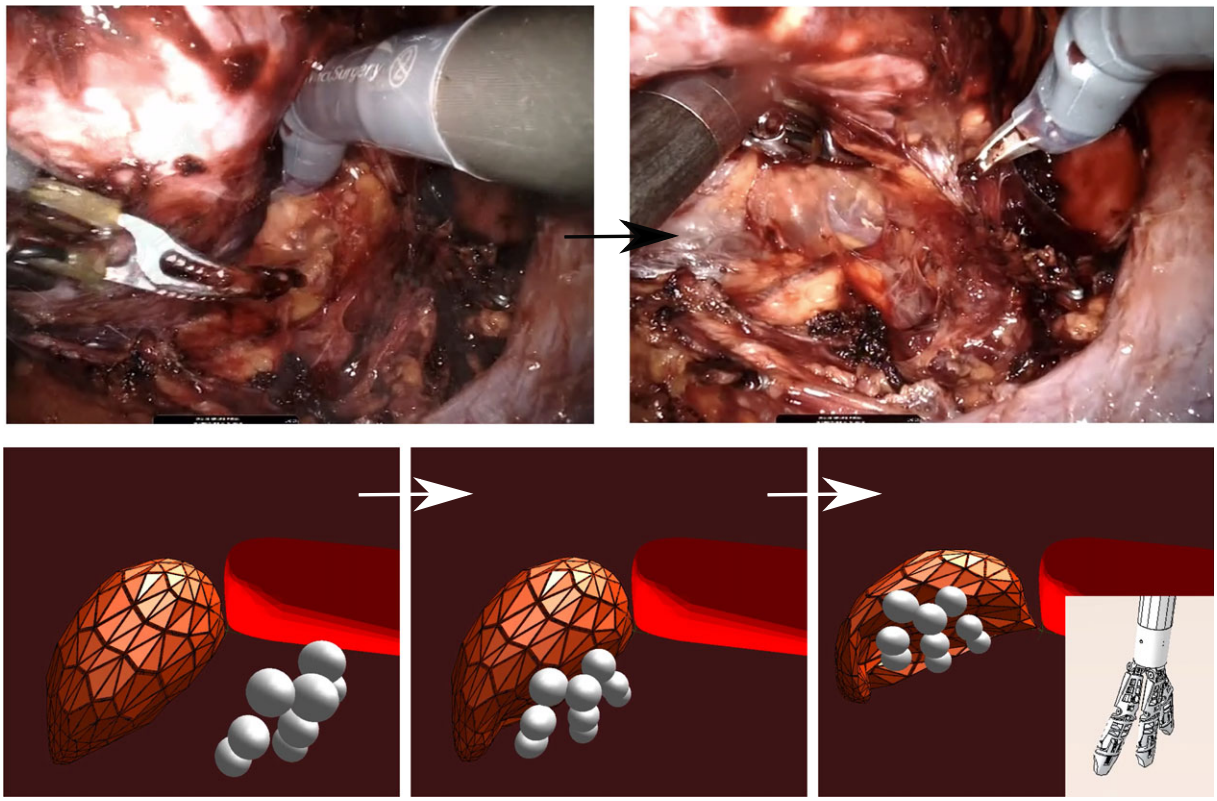

FIGURE 4 Retractor simulation. Top: real surgical procedure, Bottom: simulated environment

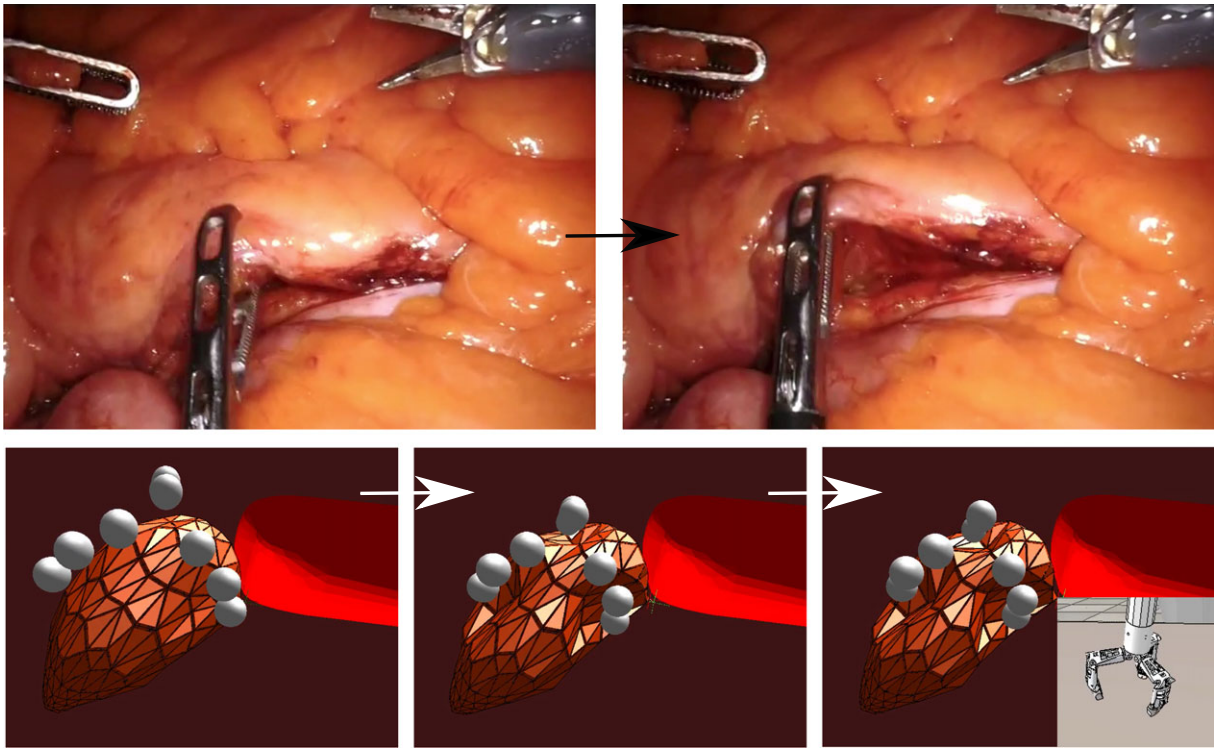

FIGURE 5 Grasp simulation. Top: real surgical procedure, Bottom: simulated environment

estimate stiffness and consistency associated with the presence of neoplasms.

Finally, Figure 6 shows the potential of MH that has a caliper by exploiting its kinematics. What represents an added value is that all these skills can be incorporated into one instrument: the MH. Changes of instruments during the intervention leads to time loss, distraction and stress for the surgeon, and higher risk of infection for the patient.

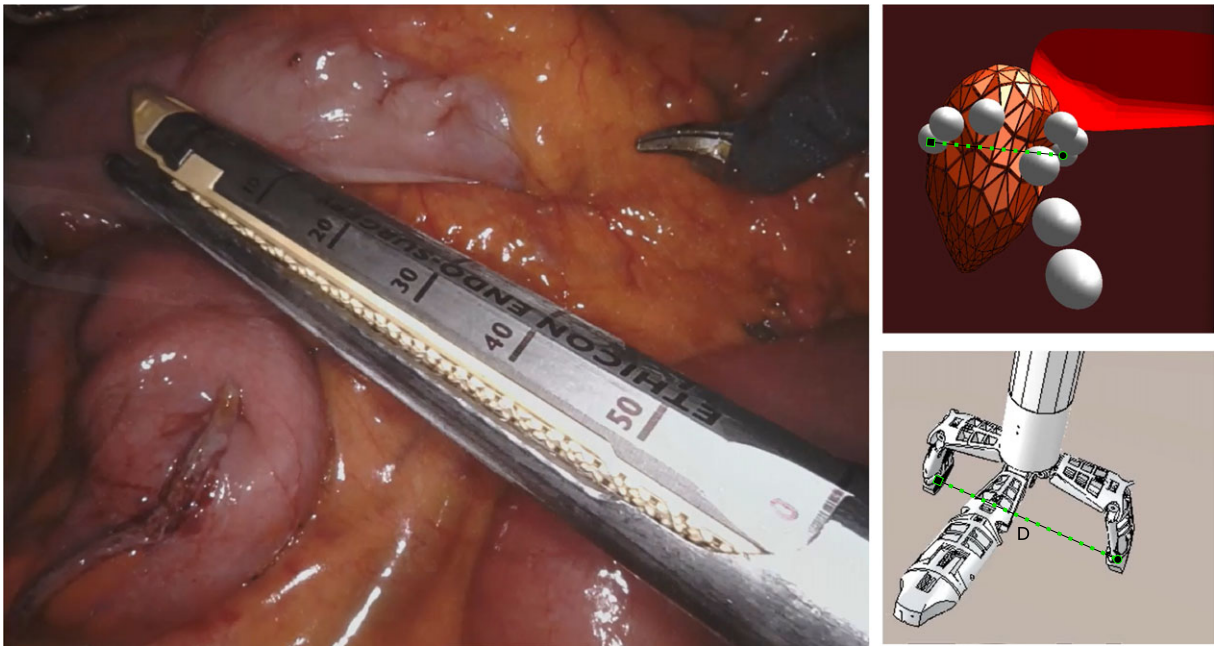

FIGURE 6 Caliper simulation. The hand direct kinematics can be used to estimate organs or tissues critical dimensions

5 | FIBER BRAGG GRATING FOR TIP SENSORS DESIGN

In this section, the design and some preliminary analysis of the proposed fiber Bragg grating (FBG)-based force sensor are shown.

In Minimally Invasive Robotic Surgery (MIRS), the loss of tactile sensation can potentially lead to tissue damage and bad execution of surgical tasks. On the contrary, feeling the force allows (a) tissue palpation for structures identification or properties/texture assessment; (b) force feedback during reconstructive procedures; (c) identification of undesired interaction between the instruments and the environment (organs) outside the viewing area; (d) development of advanced control algorithms (impedance/force control, adaptive virtual fixtures, bilateral telemanipulation control). Different solutions have been investigated in MIRS to enable patient side force estimation, eg, in Fontanelli, Buonocore, Ficuciello, Villani, and Siciliano's study,[21] a new force sensor integrated into the trocar has been developed to allow force estimation without modifying the standard laparoscopic instruments.

This solution can address the problem for most of the forceps, but it is not suitable for MH. Indeed, the tool is thought to fine manipulate objects while controlling contact forces. To allocate the force sensors in each fingertip the design should account for: (a) measurement of three components of the force, the normal, and the two tangential components; (b) miniaturization to integrate the force sensor directly into the distal phalanges; (c) simplification of the sensing element to reduce the costs and allows an easy replacement.

On the basis of these requirements, the Bragg technology has been chosen as the suitable one for sensor realization. The Bragg technology has many advantages, including miniaturization, possibility to include different sensors on the same optical fiber, high resolution, immunity to the electromagnetic interference noise, and high integration capability. In surgical scenarios, optical fibers are used in Haslinger, Leyendecker, and Seibold's study[22] to realize a six-DOF Bragg-based force sensor for a robotic laparoscopic instrument. While in Liu, Iordachita, He, Taylor, and Kang's study,[23] a subminiaturized force sensor composed of three optical fibers and based on the Fabry-Pérot interferometry method for vitreoretinal microsurgery is presented.

Our force sensor is composed of three Bragg gratings for each finger. The distal finger has been designed with a bottom part (highlighted in white in Figure 7), linked to the joint axis, and controlled by the tendon-driven mechanism. A central column with three holes is located in the finger structure: in our design, each hole is disposed at 120° one from another in which optical fiber has been glued inside.

The design choice has been evaluated using the finite element analysis (FEA) to assess the deformation of the regions in which is glued the Bragg gratings, and thus the ability of the sensor to decouple the three force components. In particular, considering the plastic material used for the prototype, a nonlinear analysis has been chosen. The results are shown in Figure 8. More in details, in Figure 8A, the stress of the structure caused by three force components (one normal and two tangential to the finger surface) of about 7 N amplitude is reported. The maximum stress is about four times smaller than the material yield stress ($4.0e^7 N/m^2$). Moreover, in Figure 8B-D, the deformation of the three Bragg fibers under one normal and two tangential components along two orthogonal directions are represented. It is possible to see that the three force components cause different deformations of the structure. However, such deformations are coupled. This means that it could be possible to find a calibration matrix that maps the three forces to the deformations of the three fibers as reported in the following.

To obtain a mathematical model that relates fiber Bragg sensors' deformations with the three forces, the measurement system shown in Figure 9 has been set up. The system is composed by two vertical holders, the one mounting the finger prototype allows three linear independent motions, and the one mounting the ATI force/torque

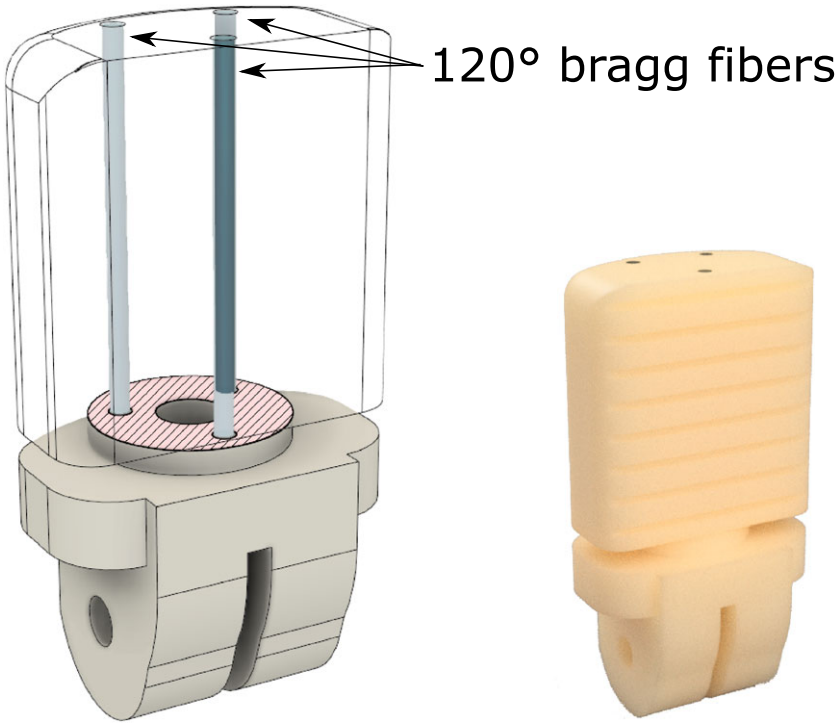

FIGURE 7 Sensor structure integrated into the distal phalanges. The section view shows the columns and the holes built to glue three Bragg fibers

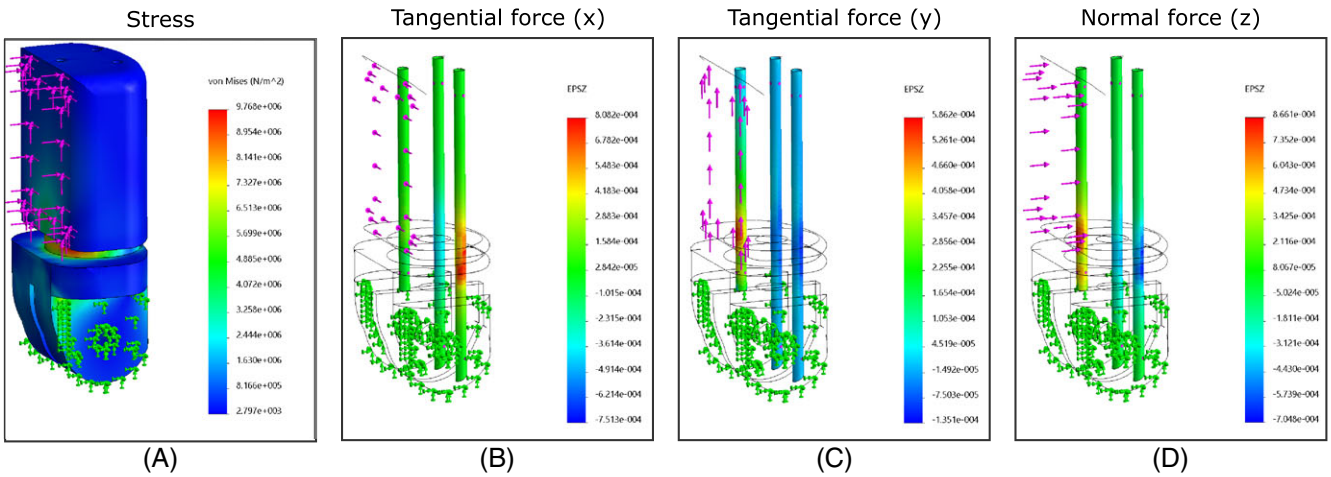

FIGURE 8 Finite element analysis of the proposed finger sensor design. A, structure stress, (B, C, D) simulated deformation of the three Bragg fibers when the phalanx is subject to a normal, tangential and vertical force

reference sensor can translate along the vertical direction. To acquire the Bragg wavelength sensors' variation, an optical sensing interrogator (Micron Optics sm130) provides the simultaneous interrogation of the sensors.

By acquiring a sufficient number of measurement variations of Bragg wavelength related to forces applied along *x*, *y*, and *z* axis, it is possible to obtain the 3 × 3 coefficient matrix

$$\begin{bmatrix} F_x \\ F_y \\ F_z \end{bmatrix} = \begin{bmatrix} A_1 & B_1 & C_1 \\ A_2 & B_2 & C_2 \\ A_3 & B_3 & C_3 \end{bmatrix} \begin{bmatrix} \Delta\lambda_1 \\ \Delta\lambda_2 \\ \Delta\lambda_3 \end{bmatrix}, \tag{8}$$

The vertical holder allows controlling motions along the three axes with very high precision to stimulate a pressure on the prototype finger that perfectly fits a rigid support designed on purpose and attached to the reference sensor (Figure 10). Thus, the system allows applying forces along single directions with increasing intensity, obtaining a sufficient number of measurements contained in a suitable range.

A fiber Bragg sensor consists of a periodic modulation of the refractive index in the core of a single-mode optical fiber. When the light from a broadband source is launched from one side of the fiber, only a particular wavelength that satisfies Bragg condition is reflected while the remainder is transmitted without any loss.[24] It can also be demonstrated that the reflectivity is a function of the grating length. Thus, fiber gratings are excellent elements in sensing applications.[25] The operating principle is to monitor the shift in Bragg wavelength related to the changes in the measure. The Bragg wavelength is a

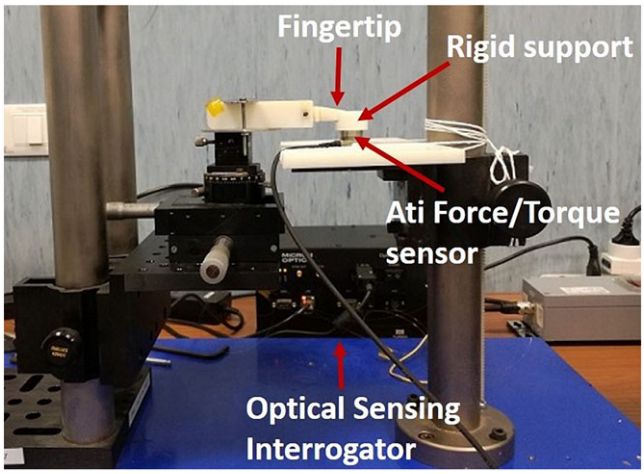

FIGURE 9 Measurement system

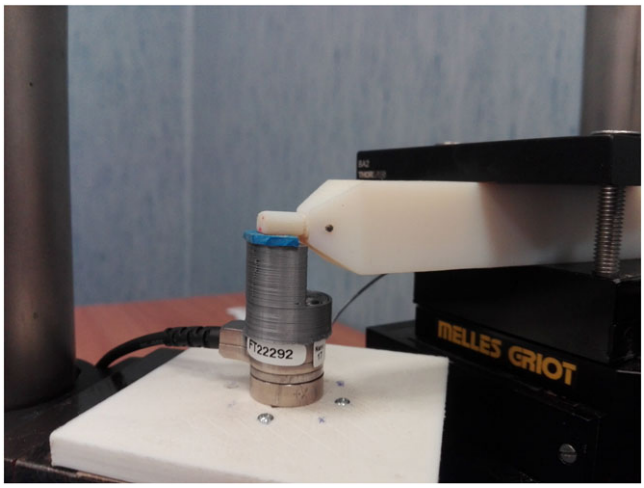

FIGURE 10 A detailed view of the prototype finger and the reference sensor

function of the grating period Λ and the effective refractive index n_{eff} of the fiber core

$$\lambda_B = 2n_{eff}\Lambda. \tag{9}$$

Any change in the refractive index or the grating period because of external measure changes the Bragg wavelength and can be detected.[26] In this experiment, the strain variation is the parameter that directly tunes the center wavelength of the Bragg grating. Because of the wavelength-based working principle of Bragg-sensing technology, the measure is not affected by the amplitude variation of the light emission caused by fiber bending outside the Bragg zone.[27] This makes FBG technology suitable for force measurements even when the fiber is bending inside the MH joints. In a first experience, the Bragg wavelength and the relative mechanical variation along *z*-axis have been simultaneously acquired obtaining a sample of 10 measurements for different values of the force. Afterward, data have been manipulated via MATLAB to calculate the best linear fit and to extract the coefficients related to the sensor characteristic (Figure 11).

To prove the effectiveness of the FBG sensor, we have compared 10 measurements of the force component along *z*-axis measured by

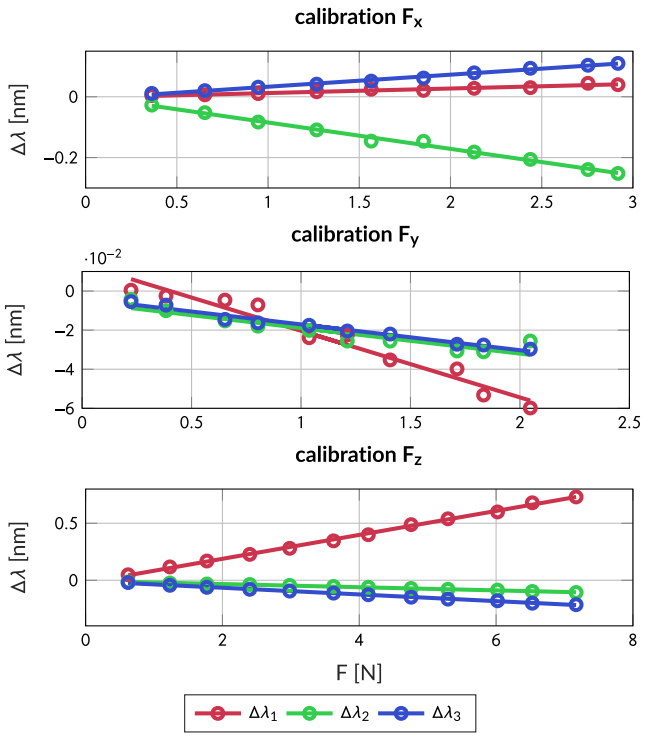

FIGURE 11 Coefficients associated with the sensor characteristic

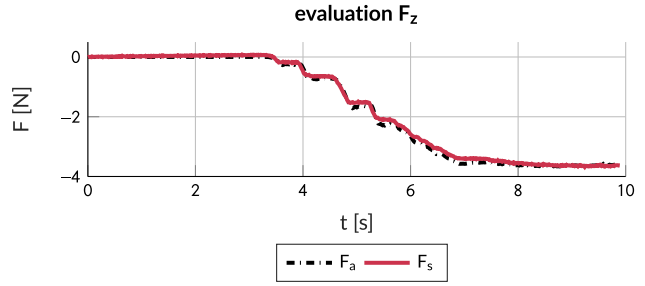

FIGURE 12 Force measure evaluation along z axis. F_a:ati force, F_s:sensor force

the ATI sensor and the FBG sensor (see Figure 12). The percentage error associated with the average carried out on the measurements is less than 5%.

6 | THE MUSHA PROTOTYPE

In this section, the design choices and the first prototype of MH are shown.

6.1 | Requirements and design choice

The design requirements have been identified in collaboration with the surgeons and taking into account the constraints due to the da Vinci configuration for the tools. The desiderata are described in the following:

- To comply with the task requirements, the tool should have a high number of DOFs that allow complex and human-like motions.

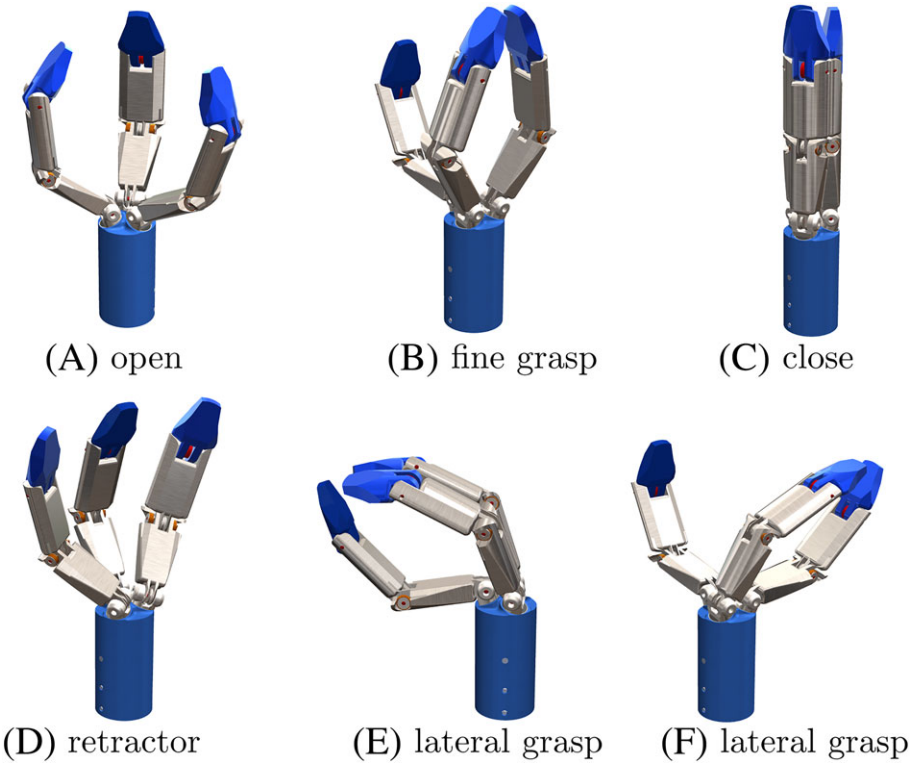

FIGURE 13 The hand prototype with the motors box

- A unified instrument that allows simultaneous tissue traction and manipulation and can act as a retractor to gently manipulate organs is needed.
- The instrument should provide the ability to perform both fine (needle and thread grasp) and power grasp (even for considerably large anatomical parts).
- The capability to perform dexterous movements while in contact with the tissue (eg, torsion or rolling) would contribute to the diagnosis phase.
- To be used as an instrument of the da Vinci robotic platform, the robotic hand has to pass through the trocar, and a restriction on the maximum number of actuators is necessary.

According to the requirements, we have chosen the hand dimension reported in Figure 13. In this first prototype, the instrument diameter is of 15 mm that is still not adequate for the da Vinci robot since the trocar is of 13 mm. The phalanges' length has been chosen according to existing tools like the Storz retractor. To switch among different hand configuration: power grasp, fine grasp, retractor (see Figure 14), the mechanism is composed by two shafts, linked at the base of the index and medial phalanges, and free to rotate because of the presence of a couple of bearings. The two joints' axes are designed to form 20ř with respect to the central axis of the instrument. Two conical gears are linked to each shaft to guarantee an opposite and coupled motion. Moreover, another conical gear was linked to the instrument shaft with its axis orthogonal to the instrument axis and is designed to engage with the other two conical bearings perfectly. Finally, this last conical bearing is actuated by a couple of tendons in antagonistic configuration. This solution allows rotating and opening the medial and index fingers to obtain the retractor configuration as represented in Figure 11D.

Based on the requirements, we have developed a conceptual computer-aided design (CAD) solution for the MH. The tendon configuration reported in Figure 15 has been considered. More in details, in each finger, the proximal finger is actuated by a couple of tendons in an antagonistic configuration; the medial finger rotation is obtained by a single tendon resorting to two springs to obtain the antagonistic motion. Moreover, the medial and the distal fingers are coupled using a couple of tendons linked to the distal finger pulley in an antagonistic way and crossed. The described mechanism permits the rotation of the distal finger coupled with the rotation of the medial finger and scaled of a value equal to the pulleys ratio, about 70% to implementing the human-inspired ratio between the medial and distal phalanges.

Hence, for each finger, we have one actuation in antagonistic configuration composed by two tendons (green in Figure 15) and a single tendon to move the coupled medial and distal fingers (purple in Figure 15). Additionally, two other tendons in antagonistic configuration are used to actuate the reconfiguration mechanism (retractor configuration).

6.2 | Prototype

In Figure 13, the scale model prototype used for the experiments is shown. More in details, it is composed by a box containing motors, control, and electronic actuation boards. The 2 : 1 scaled hand has been printed in plastic using the PolyJet process.* About the actuation, 4 servomotor Tower Pro MG995 are chosen considering the torque

*http://www.stratasys.com/3d-printers/design-series/objet24

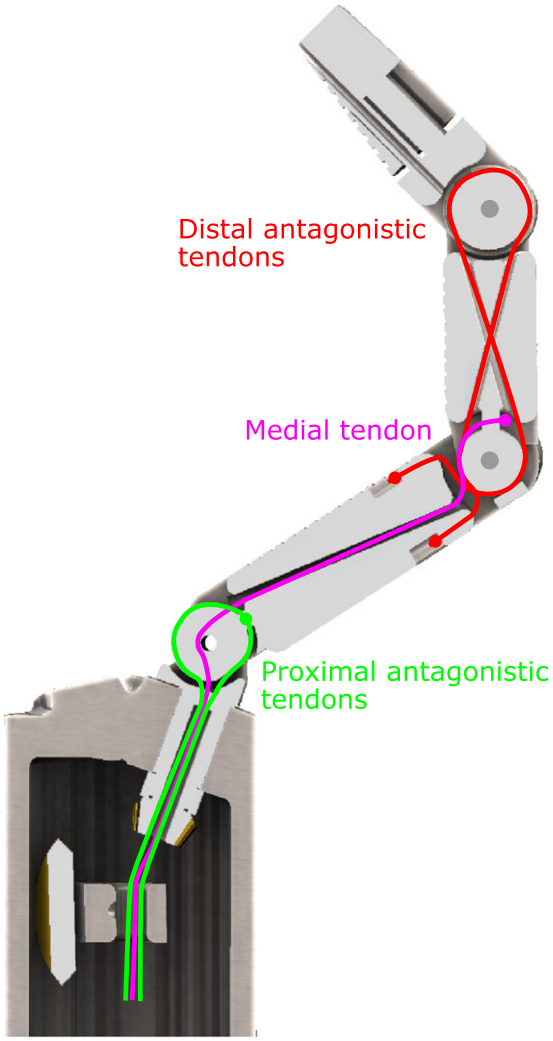

FIGURE 14 The hand configurations

(1.1 Nm) that they can produce. We have found that a torque of 1 Nm on all joints is enough to move the hand and to guarantee a maximum force on each distal phalanges of about 5 N in the worst case. The motors are controlled using Arduino DUE micro-controller. A MATLAB software has been developed to implement all the algorithms described in Section 4.

7 | CONCLUSIONS AND FUTURE PERSPECTIVES

In this paper, preliminary results on a three-fingered surgical hand have been described with the aid of experiments and simulations. Taking advantage of interviews with surgeons and working side by side with them, design specifications have been retrieved from their experience and advice. Three kinematic solutions have been evaluated using cost functions based on the concept of controllable internal forces and controllable motions. Among the three proposed solution, preliminary investigations have identified the one that optimizes grasping and manipulation capabilities. Furthermore, a prototype has been realized with 3D printing technology for testing the first kinematic solution and the fingertip force sensor solution based on FBG technology. Future work will focus on the realization of a metal prototype in a 1:1 scale that can be mounted and tested on the da Vinci Research Kit. According to surgeons' feedback, this anthropomorphic tool holds excellent potential in LS as a retractor that can be reconfigured to address different tasks where dexterity makes the difference. Moreover, the tool can be used as a caliper for different purposes as explained in Section 3 and, thanks to the force measurements, as a probe for organ/tissue palpation.

ORCID

Mario Selvaggio https://orcid.org/0000-0002-2460-1914

REFERENCES

1. Kavic MS. Hand-assisted laparoscopic surgery - HALS. *J Soc Laparoendoscopic Surg*. 2001;5(2):101-103.
2. Ikuta K, Hasegawa T, Daifu S. Hyper redundant miniature manipulator "hyper finger" for remote minimally invasive surgery in deep area. In: IEEE International Conference on Robotics and Automation; 2003; Taipei, Taiwan:1098-1102.
3. Cavusoglu MC, Williams W, Tendick F, Sastry SS. Robotics for telesurgery: second generation Berkeley/ucsf laparoscopic telesurgical workstation and looking towards the future applications. *Ind Robot: An Int J*. 2003;30(1):22-29.
4. Lum MJH, Trimble D, Rosen J, et al. Multidisciplinary approach for developing a new minimally invasive surgical robotic system. In: IEEE/RAS-EMBS Int. Conf. Biomed. Robot. Biomechatoron.; 2006; Pisa, Italy:841-846.

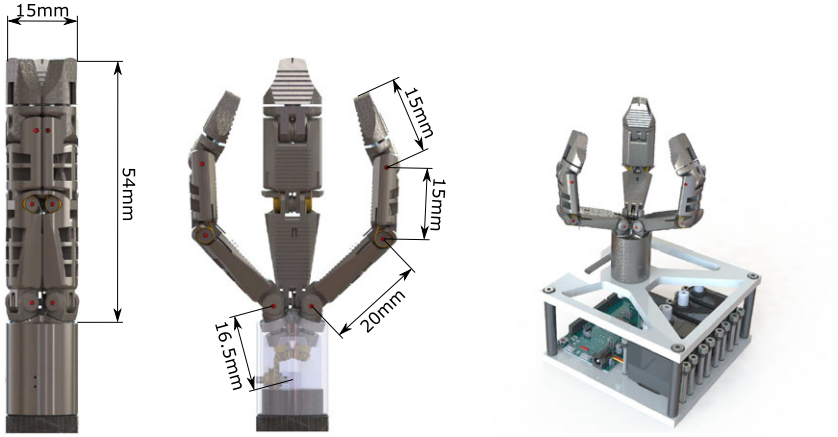

FIGURE 15 Tendon configuration

5. Tzemanaki A, Walters P, Pipe AG, Melhuish C, Dogramadzi S. An anthropomorphic design for a minimally invasive surgical system based on a survey of surgical technologies, techniques and training. *Int J Med Rob Comput Assisted Surg*. 2014;10(3):368-378.
6. Luo H, Wang S. Multi-manipulation with a metamorphic instrumental hand for robot-assisted minimally invasive surgery. In: The 2011 IEEE/ICME International Conference on Complex Medical Engineering; 2011:363-368.
7. Bracale U, Lazzara F, Merola G, Andreuccetti J, Barone M, Pignata G. Single access laparoscopic left hemicolectomy with or without inferior mesenteric artery preservation: our preliminary experience. *Minerva Chirurgica*. 2013;68(3):315-320.
8. Bracale U, Azioni G, Rosati M, Barone M, Pignata G. Deep pelvic endometriosis (adamyan iv stage): multidisciplinary laparoscopic treatments. *Acta Chirurgica Iugoslavica*. 2009;56(1):41-46.
9. Stevenson A, Solomon M, Lumley J, et al. Effect of laparoscopic-assisted resection vs open resection on pathological outcomes in rectal cancer: the alacart randomized clinical trial. *JAMA*. 2015;314(13):1356-1363.
10. Morelli L, Guadagni S, Mariniello MD, et al. Robotic giant hiatal hernia repair: 3 year prospective evaluation and review of the literature. *Int J Med Rob Comput Assisted Surg*. 2015;11(1):1-7.
11. Toh JWT, Zakaria A, Yang I, Kim SH. Totally robotic single docking low anterior resection for rectal cancer: pearls and pitfalls. *Tech Coloproctology*. 2017;21(11):893-895.
12. Santello M, Flanders M, Soechting J. Postural hand synergies for tool use. *J Neurosci*. 1998;18(23):10105-10115.
13. Palli G, Melchiorri C, Vassura G, et al. The dexmart hand: mechatronic design and experimental evaluation of synergy-based control for human-like grasping. *Int J Rob Res*. 2014;33(5):799-824.
14. Prattichizzo D, Malvezzi M, Gabiccini M, Bicchi A. On motion and force controllability of precision grasps with hands actuated by soft synergies. *IEEE Trans Rob*. 2013;29(6):1440-1456.
15. Prattichizzo D, Trinkle JC. *Chapter "Grasping" in the Springer Handbook of Robotics*. Berlin/Heidelberg: Springer; 2016.
16. Gabiccini M, Bicchi A, Prattichizzo D, Malvezzi M. On the role of hand synergies in the optimal choice of grasping forces. *Autom Robots*. 2011;31(2):235.
17. Malvezzi M, Gioioso G, Salvietti G, Prattichizzo D. Syngrasp: A MATLAB toolbox for underactuated and compliant hands. *Rob Autom Mag, IEEE*. 2015;22(4):52-68.
18. Rohmer E, Singh SPN, Freese M. V-REP: A versatile and scalable robot simulation framework. In: 2013 IEEE/RSJ International Conference on Intelligent Robots and Systems; 2013:1321-1326.
19. Fontanelli GA, Selvaggio M, Ferro M, Ficuciello F, Vendiuelli M, Siciliano B. A V-REP simulator for the da Vinci research kit robotic platform. In: 2018 7th IEEE International Conference on Biomedical Robotics and Biomechatronics (Biorob); 2018:1056-1061.
20. Fazioli F, Ficuciello F, Fontanelli GA, Siciliano B, Villani L. Implementation of a soft-rigid collision detection algorithm in an open-source engine for surgical realistic simulation. In: IEEE Int. Conf. on Robotics and Biomimetics; 2016; Piscataway, NJ:2204-2208.
21. Fontanelli GA, Buonocore LR, Ficuciello F, Villani L, Siciliano B. A novel force sensing integrated into the trocar for minimally invasive robotic surgery. In: 2017 IEEE/RSJ International Conference on Intelligent Robots and Systems (IROS); 2017:131-136.
22. Haslinger R, Leyendecker P, Seibold U. A fiberoptic force-torque-sensor for minimally invasive robotic surgery. In: 2013 IEEE International Conference on Robotics and Automation; 2013; Karlsruhe, Germany:4390-4395.
23. Liu X, Iordachita II, He X, Taylor RH, Kang JU. Miniature fiber-optic force sensor for vitreoretinal microsurgery based on low-coherence Fabry-Pérot interferometry. *Proc SPIE–Int Soc Opt Eng*. 2013;8218(5):82180O.
24. Kashyap R, Higuera JML. *Handbook of Optical Fiber Sensing Technology*. New York, NY: John Wiley and Sons; 2002.
25. Kashyap R. Chapter 1 - introduction. In: Kashyap R, ed. *Fiber Bragg Gratings*, 2nd ed. Boston: Academic Press; 2010:1-13.
26. Kawasaki BS, Hill KO, Johnson DC, Fujii Y. Narrow-band bragg reflectors in optical fibers. *Opt Lett*. 1978;3(2):66-68.
27. Saccomanno A, Laudati A, Szillasi Z, et al. Long-term temperature monitoring in CMS using fiber optic sensors. *IEEE Sens J*. 2012;12(12):3392-3398.

How to cite this article: Selvaggio M, Fontanelli GA, Marrazzo VR, et al. The MUSHA underactuated hand for robot-aided minimally invasive surgery. *Int J Med Robotics Comput Assist Surg*. 2019;e1981. https://doi.org/10.1002/rcs.1981